Underlying Mechanism of Time Dependent Surface Properties of Calcite ($CaCO_3$): A Baseline for Investigations of Reservoirs Wettability

Chia-Yun Lai,[†,∥] Monica Cozzolino,[‡,∥] Maria Vittoria Diamanti,[‡] Saeed Al Hassan,[§] and Matteo Chiesa*[,†]

[†]Institute Center for Energy (iEnergy), Masdar Institute of Science and Technology, Abu Dhabi, United Arab Emirates

[‡]Dipartimento di Chimica, Materiali ed Ingegneria Chimica 'G. Natta', Politecnico di Milano, 20133 Milano, Italy

[§]Department of Chemical Engineering, Petroleum Institute, Abu Dhabi, United Arab Emirates

Received: October 29, 2015
Revised: December 7, 2015
Published: December 10, 2015

Corresponding Author
*M. Chiesa. E-mail: mchiesa@masdar.ac.ae.

INTRODUCTION

Water flooding is widely used in the oil industry for its efficiency and economic feasibility.[1] Advantages such as maintaining reservoir pressure above the oil's bubble point pressure and improving viscous flow in porous media make water flooding the dominating secondary recovery strategy. On the basis of this fact, knowing the properties of the reservoir is important to enhance the efficiency of water flooding technique. One of the key factors that affects the success of water flooding processes can be attributed to wettability of porous surfaces within reservoir rocks.[2] The common scenario one may encounter in the oil recovery operation is facing the complexity of the physical morphology and the chemical composition of the porous core. The former involves parameters including permeability, pore connectivity, and pore size distribution in the reservoir, whereas the latter relates to the molecular interactions between the different phases crude oil, brine and rock (CBR). Although studies on the influence of wettability on oil recovery and waterflood performance have been extensively performed by various research groups,[2−6] a conclusive and satisfactory understanding of all the parameters, depending both on the intrinsic properties of the material composing the reservoir and on the extrinsic conditions that the reservoir has been subjected to, has not yet been completely achieved.

Low water wetting behavior of the carbonate reservoir's rocks causes unfavorable average oil recovery to less than 30% with a water flooding technique.[1] Adjusting the injected water ionic composition has been shown to impact the CBR wetting properties,[7−9] resulting in reservoir wettability inversion toward more water wet. Furthermore, it has been proven that by altering the wettability to a slightly water wet scenario, increasing oil recovery of the carbonate reservoirs can be realized.[10] The efficiency of wettability inversion depends on the reservoir's geological classification,[11] thermodynamic conditions,[12,13] and the crude oil's acidic and basic components.[14−16] However, to date, the fundamental chemical understanding of these interactions remains elusive.[1] Together with a great variety of reservoirs and crude oil properties worldwide, the quantitative results from one reservoir are inapplicable for the other reservoirs. In light of this concern, it is inadequate to merely perform state of the art experiments in one specific reservoir environment, as we also have to interpret the physical science behind the sequential results that enable us to predict the outcomes of the other reservoirs. Macroscopic techniques such as static and dynamic contact angle measurements or nuclear magnetic resonance[17−19] fail to provide information for the wetting behavior within the pore due to the lack of spatial resolution, hinting higher spatial resolution measurements are needed. Moreover, the resolution needs to be comparable to or finer than pore sizes, i.e., submicrometer to micrometer range. Serving as the indispensable intermediary to improve the ultimate performance of flooding techniques,

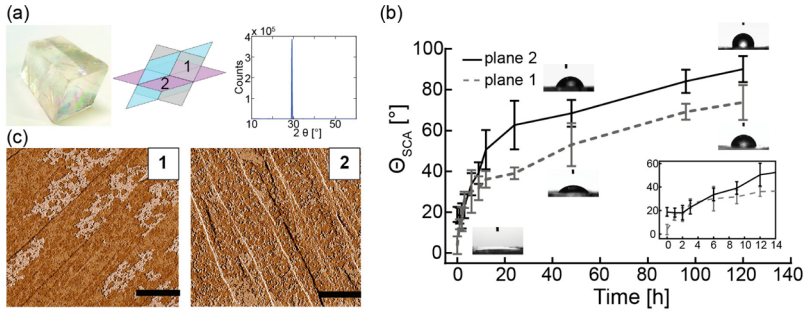

Figure 1. (a) Illustration for the representation of 2 cleavage planes. (b) Time dependent SCAs for plane 1 and plane 2. (c) AFM phase image for 2 calcite cleavage planes. Scale bar: 500 nm.

nanoscale observations enable researchers to tackle the challenges with better understanding in pore surface properties.

To simplify the complexity of the system, we start by investigating an atomically flat surface of mineral composition representative for carbonate type formation. Calcite ($CaCO_3$) is the most common carbonate mineral and the most stable polymorph of calcium carbonate. In the petroleum reservoir, calcite is present in both shallow sea as limestone or deep water as chalk. Calcite is extensively used to represent the rock formation[20] due to the fact that it provides an idealized atomically flat surface that reduces the complex situation of a reservoir formation from morphology-chemistry coupled wettability issues to a simple chemistry related question. Due to the rhombohedric crystallographic structure of calcite, three cleavage planes can be obtained with different surface properties, which result in different wettabilities.[21] In addition to the intrinsic properties of the material, the wetting history, i.e., the calcite being wetted first by water or oil, is also expected to play an important role in determining the wettability of calcite. Furthermore, it is known that upon exposure to the environment, surface wettability undergoes a transition owing to adsorption of atmospheric contaminants.[22,23] It has already been shown by Kendall et al.[24] that freshly cleaved calcite atomically rearranges the carbonate surface in response to humid air exposure and they hypothesized in a theoretical way that the chemical species formed were hydration layers according to the substrate structure and associated electrostatic potential. Yet, with abundant literature on calcite surface properties in hand, wettability of calcite is rarely discussed.

In this work, we employ macroscopic, microscopic and nanoscopic techniques, i.e., water static contact angle (SCA) measurement, dynamic atomic force microscopy (AFM) and Fourier transform infrared spectroscopy (FTIR), to examine the wettability of different calcite cleavage planes upon exposure to the atmosphere. Nanoscopic measurements enable us to observe that the development of heterogeneities on calcite surface due to surface contamination leads to wettability transition from superhydrophilic to slightly hydrophobic. Furthermore, the different growth kinetics of such heterogeneities on different calcite cleavage planes contribute to variations of SCA changing profile in time. We showed the nanoscale measurements are able to describe macroscale wettability showing that we can assess the pores wettability with improved spatial resolution approach.

EXPERIMENTAL SECTION

Calcite Sample Preparation. Calcite samples of Iceland spar variety were mechanically cleaved along the $(10\bar{1}4)$ cleavage plane with a small hammer and handled carefully to avoid contamination from the environment aside for the natural aging due to aerosol adsorption. Calcite cleaves along the unit rhombohedron labeled as plane 1 as the perfect cleavage plane. Plane 2 was determined by comparing the difference in the inclination with respect to the plane 1 as shown in Figure 1a.

Water Static Contact Angle (SCA) Measurements. The SCA measurement was obtained with a Kyowa DM-701 contact angle machine at ambient conditions, and elaborated with FAMAS (interFAce Measurement & Analyses System), the software provided by Kyowa. SCAs were measured by depositing droplets of 0.8 μL on the calcite surface. The contact angle measurements were taken at different aging times, starting form 0 h, i.e., as cleaved, then at 1, 2, 3, 6, 9, 12, 24, 48, 96, and 120 h. Aging was performed by exposing samples to the ambient conditions with 22 ± 2 °C and a water partial pressure around 1300 Pa, which corresponds to relative humidity (RH) of 50 ± 5% throughout the work. For each time step, average SCA values and standard deviations were calculated with at least 10 measurements.

Atomic Force Microscope (AFM) Force Spectroscopy Measurements. The AFM is a versatile instrument that can be used as an imaging device as well as a force measurement tool. The calcite sample was scanned with a Cypher AFM from Asylum Research and standard OLYMPUS cantilevers (AC160TS) with $k \approx 40$ N/m, $Q \approx 500$, and $f_0 \approx 300$ kHz were used. The AFM was operated in amplitude modulation mode for both image scanning and force measuring. Images were scanned in 1×1 or 2×2 μm^2 area with scan rate of 0.8 Hz. Phase imaging was employed in this work by recording the phase lag Φ of the AFM probe. For the force reconstruction method, we employed Sader–Jarvis–Katan formalism[25,26] and the detail of use is described elsewhere.[27,28] The observables amplitude A and phase lag Φ were recorded as a function of tip–sample separation distance d, i.e., APD curves. Free cantilever oscillation amplitudes of 30 nm were used to avoid bistability.[29] Furthermore, because the tip radius R is known to have a great effect on the interaction force between the tip and the surface, it has been constantly monitored in situ with critical amplitude method,[30] so that there was no change in R during the experiment. A total of 300 APD curves were collected on each cleavage plane of calcite as well as different phases on each plane for statistical analysis.

Fourier Transform Infrared (FTIR) Spectroscopy. FTIR spectroscopy is a useful tool in the molecular characterization of organic and inorganic species with quick and easy sample preparation. Calcite samples were placed in a Praying Mantis Diffuse Reflection accessory and exposed to the ambient conditions for 24 h. The accessory was mounted in the Bruker 80v FTIR spectrometer front sample compartment. All the

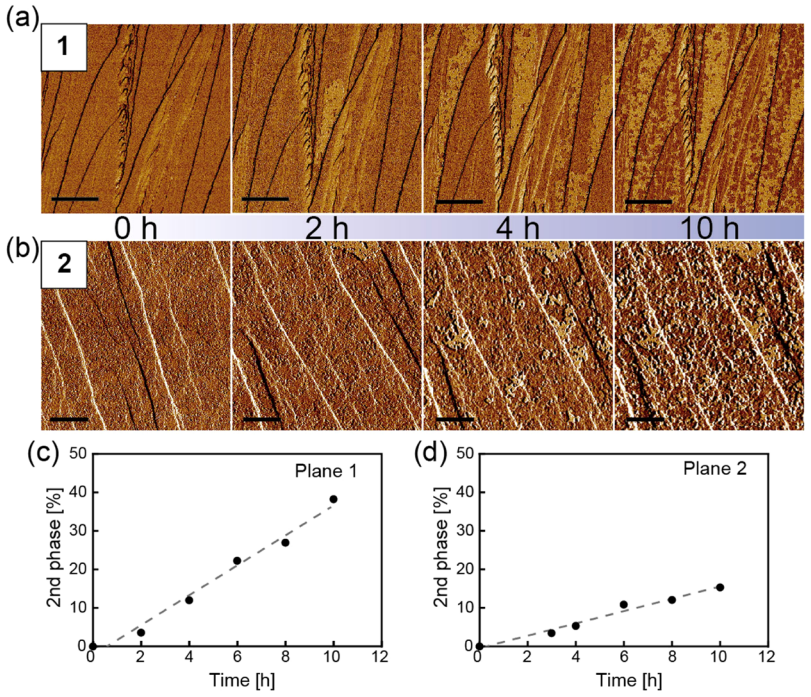

Figure 2. Time sequence AFM phase images for plane 1 (a) and plane 2 (b). (c) and (d) show the percentage of 2nd phase growing with time. Scale bar: 500 nm for (a) and 200 nm for (b).

FTIR spectra were acquired by averaging 200 scans in absorbance unit in reflective mode and using a freshly cleaved calcite surface spectrum as the baseline signal.

RESULTS AND DISCUSSION

Anisotropic crystals such as calcite are cleaved more easily and with fewer cleavage steps along some planes with respect to others.[31] Calcite $(10\bar{1}4)$ cleavage plane is confirmed with X-ray diffraction (XRD) with rotating sample stage to reduce the preferred-orientation effect. As shown in Figure 1a, a single and clear peak at ∼29.4° shows that the plane 1 we obtained corresponds to $(10\bar{1}4)$ cleavage plane. Furthermore, because a single $CaCO_3$ crystal was used, judging by the inclination of the rhombohedral crystal,[32] we could infer plane 1 and plane 2 through their macroscopic characteristic, i.e., the angle of 74.9° between adjacent plane 1 and plane 2.

Macroscopic measurements to evaluate the wettability of calcite when exposed to ambient conditions were first carried out with SCA sessile drop method. As shown in Figure 1b, freshly cleaved calcite plane 1 exhibited a superhydrophilic property with SCA smaller than 5° whereas plane 2 showed less hydrophilic behavior with SCA ∼ 18.9 ± 3.7°. To avoid ambiguity, we defined t = 0 h when calcite was freshly cleaved for both planes. Upon aging, SCAs of both planes increased and reached ∼73.8 ± 8.5° for plane 1 and ∼90 ± 6.4° for plane 2 after 120 h of cleaving. The wettability transition of these two planes shared similar trend, yet yielded more hydrophobic for plane 2, indicating plane 2 has smaller surface energy than plane 1. Furthermore, the appearance of a wettability transition suggests that the surface properties of these 2 cleavage planes varied as they were exposed to the environment, either morphologically or chemically. AFM scanning was carried out to examine the calcite surfaces and the root-mean-square (RMS) roughness was calculated. The RMS roughness difference between as cleaved conditions and after 24 h exposure is 50 pm for plane 1 and 20 pm for plane 2, showing the morphological variation is negligible and cannot be responsible for such wettability alteration. Nonetheless, AFM phase imaging, which provides information on the surface chemical composition,[33] presented contrasts. Figure 1c shows the AFM phase images of the 2 cleavage planes at t = 6 h. The contrast presented in Figure 1c shows that within each plane, different portions of the surface dissipate energies differently,[34] implying the formation of chemistry heterogeneity on freshly cleaved calcite as a consequence of exposure to ambient conditions. Therefore, the wettability of calcite is showed to be affected by both the intrinsic characteristics, i.e., crystallographic planes, as well as by external conditions such as exposure time to the environment.

To further study the development of chemistry heterogeneity when calcite surfaces were exposed to the environment, we recorded the phase contrasts of the AFM scan with aging time, i.e., from t = 0 h to t = 10 h. As shown in Figure 2a,b, no contrast was present in phase images at t = 0 h in both planes: we called this state the first phase, which is representative of pure calcite. With time elapsed, another phase emerged in the form of lighter color: we called it the second phase. In the figure, we can see that the second phase evolved differently on plane 1 and plane 2. In the former case it established from the surface steps edges and formed more continuous patches over the scanned area, whereas on plane 2 it appeared randomly dispersed on the surface and scattered all over the plane. The kinetics of the second phase development on different planes were evaluated by quantifying the occupied area and normalizing on the whole scanned area. As shown in Figure 2c,d, the increase in the second phase percentage belongs to zero-order kinetics; i.e., its surface coverage increases linearly, both with R^2 > 0.97 and with slope 3.88 on plane 1 and 1.60 on plane 2. We observed that both the growth rate and the pattern of the second phase varied with different calcite cleavage planes, thus confirming the complexity of the oil reservoirs wettability

investigations. The presence of surface heterogeneity strengthens the need for micro- to nanoscale understanding of the surface properties.

AFM force spectroscopy technique was also performed aiming to quantify how the calcite surface properties changed when the second phase appeared. AFM tip−sample force profiles were reconstructed with either the first phase or the second phase present on two planes. As shown in Figure 3a,c,

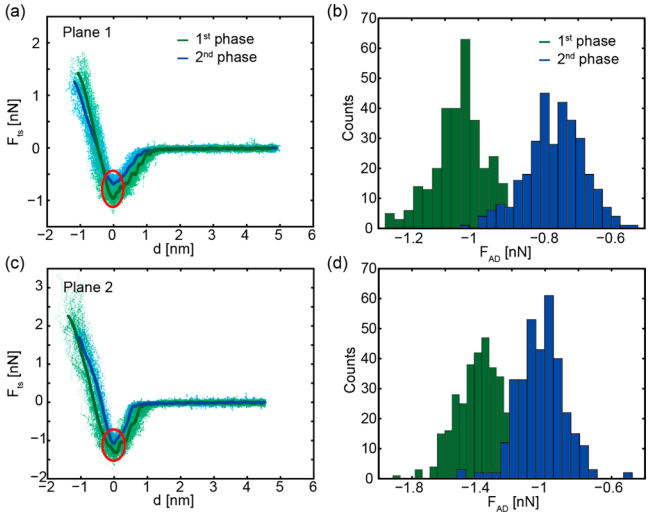

Figure 3. (a) Force profiles for both phases on plane 1. (b) Histogram of F_{AD} for the first and second phase one plane 1. (c) Reconstructed force curves on plane 2. (d) F_{AD} histogram for both phases on plane 2. Blue and green dots represent for experimental data, and the continuous lines stand for averaged force curves.

on both planes two distinct profiles were recorded as a function of the different phase investigated. The absolute values of minimum force in the force profiles are extracted from the experimental data and defined as adhesion force (F_{AD}). The magnitude of F_{AD} depends on the AFM tip radius and sample surface chemistry, and F_{AD} can be expressed as[35]

$$F_{AD} = -\frac{R_{tip}H}{6a_0^2} \tag{1}$$

where R_{tip} is the tip radius, H is the Hamaker constant, and a_0 is the intermolecular distance. The difference in the adhesion force F_{AD} can be clearly seen in Figure 3b,d. Bimodal distribution is examined by Hartigan's dip test showing significance bimodality[36] and could be observed in both plots and the difference of these two populations is meaningful with statistical analysis.[37] Because R_{tip} was monitored throughout the experiments ensuring no change occurred, F_{AD} here is then solely affected by sample surface properties. In other words, the two phases present on the calcite surfaces are chemically different. AFM force measurements are in agreement with AFM phase images showing that as freshly cleaved calcite is exposed to the ambient conditions, chemistry heterogeneity develops and consequently changes the surface properties.

Furthermore, F_{AD} between the AFM probe and the calcite surface can also be expressed by using the sphere-flat plane model:[35,38]

$$|F_{AD}| = 4\pi R_{tip}\gamma \tag{2}$$

where γ is the surface energy. Together with the second phase growth rate presented in Figure 2c,d, we estimated the change in effective adhesion force F_{AD} and then we normalized the change with respect to the F_{AD} value at $t = 0$ h to disregard the uncertainty in evaluating the true value of R_{tip}. That is, we can write the effective F_{AD} as

$$F_{ij}^* = \frac{|F_{AD,ij}|}{|F_{AD,i0}|} = \frac{\gamma_{ij}}{\gamma_{i0}} \tag{3}$$

where F_{ij}^* stands for normalized effective F_{AD} at cleavage plane i and time j. In terms of macroscopic measurements, by recalling Young−Dupré relation, we have

$$W = \gamma_L(1 + \cos\theta) \tag{4}$$

where W is the work of adhesion, γ_L is the surface energy of water, and θ is the contact angle. Again we normalized the change regarding to $1 + \cos\theta$ value at $t = 0$ h so that we could compare the results in macro- and nanoscale. In other words, the normalized macroscale parameter W can be written as

$$W_{ij}^* = \frac{W_{ij}}{W_{i0}} = \frac{(1 + \cos\theta_{ij})}{(1 + \cos\theta_{i0})} \tag{5}$$

where W_{ij}^* represents normalized work of adhesion of plane i and time j. In Figure 4a, by plotting normalized effective F_{ij}^* together with W_{ij}^*, we could see the macroscale and nanoscale measurements show good agreement in plane 1 with linear regression test showing that the slopes had no significance difference. W_{ij}^* measures macroscopically the strength of the water contact whereas F_{ij}^* captures at the nanoscale the surface properties variation in terms of adhesion forces. Nevertheless, as F_{ij}^* is able to depict the surface wettability as W_{ij}^*, one of the advantages F_{ij}^* holds is to study the calcite surface with higher spatial resolution. In Figure 4b, macro- and nanoscale measurements share a less similar trend with slopes being extremely significant. This dissimilarity can be expected because the randomly distributed second phase development could lead to higher surface energy variance.

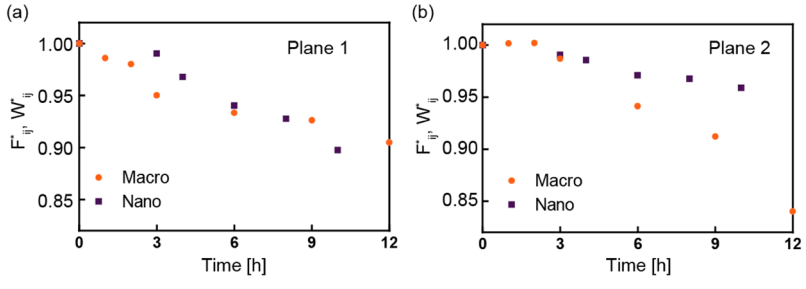

Figure 4. Macroscopic and nanoscopic measurements trend in plane 1 (a) and plane 2 (b).

FTIR experiments were then performed to investigate the second phase composition. Newly cleaved calcite plane 1 was subjected to mid-IR beam and then was left exposed to the ambient air. The spectrum at t = 0 h was taken as the baseline signal and the change of the spectra after 24 h of exposure was evaluated: the increase in spectra peaks intensity will serve as the proof for surface composition variation. Figure 5 shows the

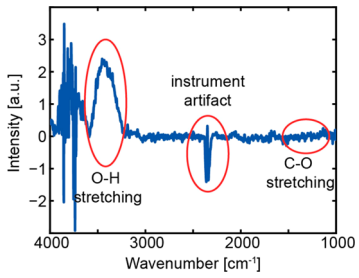

Figure 5. FTIR spectrum shows the change in peaks intensity of aged calcite plane 1.

absorbance spectra of plane 1 with the instrument artifact signal in 2400 cm^{-1}, which fluctuated in every measurement independent of users and samples. It is evident that the only variance in the spectrum falls in 3200−3600 cm^{-1}, which belongs to O−H stretching signal. On the contrary, the C−O bending and stretching vibrations of calcite characteristic peak[39] in 1420 cm^{-1} show no difference. The increase in O−H bonding signal could be the result of loosely bound water on the surface as reported earlier.[24] To reach thermodynamic equilibrium, freshly cleaved calcite adsorbs water from the humid air forming hydrated $CaCO_3$ to stabilize the surface.[24] Furthermore, as mentioned in eq 1, adhesion force F_{AD} is proportional to the Hamaker constant H and H of calcite−AFM tip (Si_3N_4) system varies from 1.29 zJ in a vacuum to 0.25 zJ in water. On this basis, the hydrated $CaCO_3$ could exhibit smaller F_{AD} and thus lead to smaller surface energy. This is in consistent with both macroscale (SCA) and nanoscale (AFM) measurements: when calcite surfaces are freshly cleaved, no matter which cleavage plane, they all present more hydrophilic wetting properties than the exposed surfaces.

Annealing was also carried out to further confirm the presence of hydrated $CaCO_3$ which causes the variation of calcite wettability. By heating the samples to 150 °C, we aimed to restore the initial condition of the calcite surface and remove the loosely bound water. Figure 6 shows the AFM phase imaging of both calcite plane 1 and plane 2 surfaces after subjected to annealing experiments. Contrasts in the images were removed and only the first phase was seen in the images.

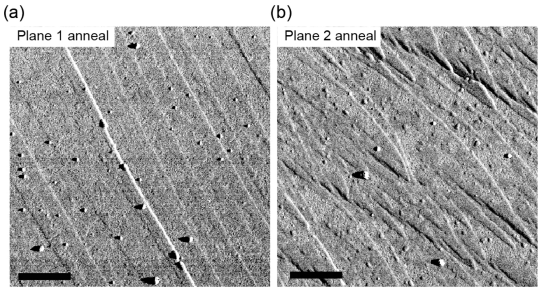

Figure 6. AFM phase image of annealed calcite plane 1 (a) and plane 2 (b) samples. Scale bar: 200 nm.

This further supports our claim that when calcite is exposed to the environment, hydrated $CaCO_3$ film is formed developing chemistry heterogeneity on the surface. Furthermore, such surface heterogeneity is responsible for calcite wettability changes with exposure time.

CONCLUSIONS

In conclusion, we have shown that the wettability of calcite depends on both intrinsic characteristics, i.e., crystallographic planes, and extrinsic conditions, i.e., wetting history, by combining SCA, AFM imaging and force measurement, and spectroscopy (FTIR) results. Freshly cleaved calcite undergoes the wettability transition from superhydrophilic/hydrophilic to hydrophobic after exposure to ambient conditions for 120 h by adsorbing water from the environment and forming hydrated $CaCO_3$. The growth kinetics and patterns of the hydrated $CaCO_3$ film varies as a function of different cleavage planes and thus contributes to the diverse wettability of calcite. The presence of hydrated $CaCO_3$ film is supported by FTIR spectra and could be removed by annealing the samples. From the results reported here, a macroscopic measurement alone, i.e., SCA, is insufficient to understand how the wettability of calcite varies with time and to understand the causes. Corroborating nanoscale measurements allow us to study calcite surface properties with finer spatial resolution. We believe our work presented here establishes a baseline for calcite wettability investigation and can be applied to future study of the composition of injected water to enhanced oil recovery.

Author Contributions

‖Equally contributing authors.

Notes

The authors declare no competing financial interest.

ACKNOWLEDGMENTS

The authors thank Dr. Marios Katsiotis for assistance in XRD experiments, and Maritsa Kissamitaki for graphic preparation. In addition, the authors also thank Dr. Sergio Santos, Ayoola Brimmo, and Carlo Alberto Amadei for useful discussion and comments of the experimental details and manuscript writing.

REFERENCES

(1) Sheng, J. J. *Enhanced Oil Recovery Field Case Studies*, 1 ed.; Gulf Professional Publishing: Waltham, MA, 2013.

(2) Anderson, W. G. Wettability Literature Survey-Part 6: The Effects of Wettability on Waterflooding. *JPT, J. Pet. Technol.* **1987**, *39*, 1605−1622.

(3) Craig, F. F. *The Reservoir Engineering Aspects of Waterflooding*; H. L. Doherty Memorial Fund of AIME: New York, 1993.

(4) Morrow, N. R.; Lim, H. T.; Ward, J. S. Effect of Crude-Oil-Induced Wettability Changes on Oil Recovery. *SPE Form. Eval.* **1986**, *1*, 89−103.

(5) du Petrole, F.; Malmaison, F. R. Evaluation of Reservoir Wettability and Its Effect on Oil Recovery. In *Interfacial Phenomena in Petroleum Recovery*; CRC Press: Boca Raton, FL, 1990; p 319.

(6) Karabakal, U.; Bagci, S. Determination of Wettability and Its Effect on Waterflood Performance in Limestone Medium. *Energy Fuels* **2004**, *18*, 438−449.

(7) Al-Mjeni, R.; Arora, S.; Cherukupalli, P.; Van Wunnik, J.; Edwards, J.; Felber, B. J.; Gurpinar, O.; Hirasaki, G. J.; Miller, C. A.;

Jackson, C. Has the Time Come for EOR? *Oilfield Rev.* **2010**, *22*, 16−35.
(8) Fathi, S. J.; Austad, T.; Strand, S. Effect of Water-Extractable Carboxylic Acids in Crude Oil on Wettability in Carbonates. *Energy Fuels* **2011**, *25*, 2587−2592.
(9) Buckley, J. S.; Liu, Y. Some Mechanisms of Crude Oil/Brine/Solid Interactions. *J. Pet. Sci. Eng.* **1998**, *20*, 155−160.
(10) Jadhunandan, P. P.; Morrow, N. R. Effect of Wettability on Waterflood Recovery for Crude-Oil/Brine/Rock Systems. *SPE Reservoir Eng.* **1995**, *10*, 40−46.
(11) RezaeiDoust, A.; Puntervold, T.; Strand, S.; Austad, T. Smart Water as Wettability Modifier in Carbonate and Sandstone: A Discussion of Similarities/Differences in the Chemical Mechanisms. *Energy Fuels* **2009**, *23*, 4479−4485.
(12) Rao, D. N. Wettability Effects in Thermal Recovery Operations. *SPE Reservoir Eval. Eng.* **1999**, *2*, 420−430.
(13) Buckley, J. S.; Wang, J. Crude Oil and Asphaltene Characterization for Prediction of Wetting Alteration. *J. Pet. Sci. Eng.* **2002**, *33*, 195−202.
(14) Xie, Q.; He, S.; Pu, W. The Effects of Temperature and Acid Number of Crude Oil on the Wettability of Acid Volcanic Reservoir Rock from the Hailar Oilfield. *Pet. Sci.* **2010**, *7*, 93−99.
(15) Standnes, D. C.; Austad, T. Wettability Alteration in Chalk: 1. Preparation of Core Material and Oil Properties. *J. Pet. Sci. Eng.* **2000**, *28*, 111−121.
(16) Puntervold, T.; Strand, S.; Austad, T. Water Flooding of Carbonate Reservoirs: Effects of a Model Base and Natural Crude Oil Bases on Chalk Wettability. *Energy Fuels* **2007**, *21*, 1606−1616.
(17) Brown, R. J. S.; Fatt, I. *Measurements of Fractional Wettability of Oil Fields' Rocks by the Nuclear Magnetic Relaxation Method*. In Fall Meeting of the Petroleum Branch of AIME, 14−17 October; Society of Petroleum Engineers: Los Angeles, CA, 1956.
(18) Abdallah, W.; Buckley, J. S.; Carnegie, A.; Edwards, J.; Herold, B.; Fordham, E.; Graue, A.; Habashy, T.; Seleznev, N.; Signer, C Fundamentals of Wettability. *Technology* **1986**, *38*, 268.
(19) Yousef, A. A.; Al-Saleh, S.; Al-Kaabi, A. U.; Al-Jawfi, M. S. *Laboratory Investigation of Novel Oil Recovery Method for Carbonate Reservoirs*. In Canadian Unconventional Resources and International Petroleum Conference, 19−21 October; Society of Petroleum Engineers: Calgary, Alberta, Canada, 2010.
(20) Greenberg, M. L.; Castagna, J. P. Shear-Wave Velocity Estimation in Porous Rocks: Theoretical Formulation, Preliminary Verification and Applications1. *Geophys. Prospect.* **1992**, *40*, 195−209.
(21) Bruno, M.; Massaro, F. R.; Prencipe, M. Theoretical Structure and Surface Energy of the Reconstructed {01.2} Form of Calcite (Caco3) Crystal. *Surf. Sci.* **2008**, *602*, 2774−2782.
(22) Lai, C.-Y.; Tang, T.-C.; Amadei, C. A.; Marsden, A. J.; Verdaguer, A.; Wilson, N.; Chiesa, M. A Nanoscopic Approach to Studying Evolution in Graphene Wettability. *Carbon* **2014**, *80*, 784−792.
(23) Li, Z.; Wang, Y.; Kozbial, A.; Shenoy, G.; Zhou, F.; McGinley, R.; Ireland, P.; Morganstein, B.; Kunkel, A.; Surwade, S. P.; et al. Effect of Airborne Contaminants on the Wettability of Supported Graphene and Graphite. *Nat. Mater.* **2013**, *12*, 925−31.
(24) Kendall, T. A.; Martin, S. T. Water-Induced Reconstruction That Affects Mobile Ions on the Surface of Calcite. *J. Phys. Chem. A* **2007**, *111*, 505−514.
(25) Katan, A. J.; van Es, M. H.; Oosterkamp, T. H. Quantitative Force Versus Distance Measurements in Amplitude Modulation Afm: A Novel Force Inversion Technique. *Nanotechnology* **2009**, *20*, 165703.
(26) Sader, J. E.; Jarvis, S. P. Accurate Formulas for Interaction Force and Energy in Frequency Modulation Force Spectroscopy. *Appl. Phys. Lett.* **2004**, *84*, 1801−1803.
(27) Amadei, C. A.; Santos, S.; Pehkonen, S. O.; Verdaguer, A.; Chiesa, M. Minimal Invasiveness and Spectroscopy-Like Footprints for the Characterization of Heterogeneous Nanoscale Wetting in Ambient Conditions. *J. Phys. Chem. C* **2013**, *117*, 20819−20825.
(28) Plummer, A.; Tang, T.-C.; Lai, C.-Y.; Chiesa, M. Nanoscale Hydrophilicity Studies of Gulf Parrotfish (Scarus Persicus) Scales. *ACS Appl. Mater. Interfaces* **2014**, *6*, 16320−16326.
(29) García, R.; San Paulo, A. Amplitude Curves and Operating Regimes in Dynamic Atomic Force Microscopy. *Ultramicroscopy* **2000**, *82*, 79−83.
(30) Santos, S.; Guang, L.; Souier, T.; Gadelrab, K.; Chiesa, M.; Thomson, N. H. A Method to Provide Rapid in Situ Determination of Tip Radius in Dynamic Atomic Force Microscopy. *Rev. Sci. Instrum.* **2012**, *83*, 043707.
(31) Borc, J.; Sangwal, K. On the Perfection of Cleavage Planes of Potassium Bichromate Single Crystals. *Surf. Sci.* **2007**, *601*, 1160−1166.
(32) Rodriguez-Navarro, C.; Ruiz-Agudo, E.; Luque, A.; Rodriguez-Navarro, A. B.; Ortega-Huertas, M. Thermal Decomposition of Calcite: Mechanisms of Formation and Textural Evolution of Cao Nanocrystals. *Am. Mineral.* **2009**, *94*, 578−593.
(33) Martinez, N. F.; Garcia, R. Measuring Phase Shifts and Energy Dissipation with Amplitude Modulation Atomic Force Microscopy. *Nanotechnology* **2006**, *17*, S167.
(34) Cleveland, J. P.; Anczykowski, B.; Schmid, A. E.; Elings, V. B. Energy Dissipation in Tapping-Mode Atomic Force Microscopy. *Appl. Phys. Lett.* **1998**, *72*, 2613−2615.
(35) Israelachvili, J. *Intermolecular & Surface Forces*, 2 ed.; Academic Press: New York, 1991.
(36) Freeman, J.; Dale, R. Assessing Bimodality to Detect the Presence of a Dual Cognitive Process. *Behav Res. Methods* **2013**, *45*, 83−97.
(37) Chang, Y.-H.; Olukan, T.; Lai, C.-Y.; Santos, S.; Lin, T.-Y.; Apostoleris, H.; Font, J.; Barcons, V.; Chiesa, M. Establishing Nanoscale Heterogeneity with Nanoscale Force Measurements. *J. Phys. Chem. C* **2015**, *119*, 18267−18277.
(38) Yaminsky, V. V. The Hydrophobic Force: The Constant Volume Capillary Approximation. *Colloids Surf., A* **1999**, *159*, 181−195.
(39) Chu, D. H.; Vinoba, M.; Bhagiyalakshmi, M.; Baek, Hyun, II; Nam, S. C.; Yoon, Y.; Kim, S. H.; Jeong, S. K. Co2 mineralization into Different Polymorphs of Caco3 Using an Aqueous-Co2 System. *RSC Adv.* **2013**, *3*, 21722−21729.